Programmable Transcranial Magnetic Stimulation: A Modulation Approach for the Generation of Controllable Magnetic Stimuli

Majid Memarian Sorkhabi, Moaad Benjaber, Karen Wendt, Timothy O. West, Daniel J. Rogers, and Timothy Denison

Abstract*—*Objective: **A transcranial magnetic stimulation system with programmable stimulus pulses and patterns is presented. The stimulus pulses of the implemented system expand beyond conventional damped cosine or near-rectangular pulses and approach an arbitrary waveform.** ***Methods:*** **The desired stimulus waveform shape is defined as a reference signal. This signal controls the semiconductor switches of an H-bridge inverter to generate a high-power imitation of the reference. The design uses a new paradigm for TMS, applying pulse-width modulation with a non-resonant, high-frequency switching architecture to synthesize waveforms that leverages the low-pass filtering properties of neuronal cells. The modulation technique enables control of the waveform, frequency, pattern, and intensity of the stimulus.** ***Results:*** **A system prototype was developed to demonstrate the technique. The experimental measurements demonstrate that the system is capable of generating stimuli up to 4 kHz with peak voltage and current values of $\pm$1000 V and $\pm$3600 A, respectively. The maximum transferred energy measured in the experimental validation was 100.4 Joules. To characterize repetitive TMS modalities, the efficiency of generating consecutive pulse triplets and quadruplets with interstimulus intervals of 1 ms was tested and verified.** ***Conclusion:*** **The implemented TMS device can generate consecutive rectangular pulses with a predetermined time interval, widths and polarities, enables the synthesis of a wide range of magnetic stimuli.** ***Significance:*** **New waveforms promise functional advantages over the waveforms generated by current-generation TMS systems for clinical neuroscience research.**

***Index Terms*—IGBTs, programmable TMS, pulse shape, PWM inverter, transcranial magnetic stimulation.**

I. Introduction

TRANSCRANIAL magnetic stimulation (TMS) is an important tool used by researchers to study the central and peripheral nervous systems, and by clinicians to diagnose and treat diseases such as depression, stroke and pain. The key advantage of TMS is that it is non-invasive, and carries relatively few risks for test subjects, patients and research animals [1]. Furthermore, the choice of specific TMS stimulation parameters (e.g. timing of pulse sequences) can have either inhibitory or facilitatory effects on brain networks, including induction of long-lasting neuroplasticity [2], [3]. Repetitive TMS (rTMS) protocols, where stimulation pulses are provided in rapid succession, are also growing in popularity; but generating consecutive and constant stimuli at high rates a challenging for present-day TMS systems.

Commercially available TMS technology limits the possibilities for novel stimulation paradigms in neuroscientific experiments. Many of these limitations are inherent in the physical principles by which particular TMS technologies operate. Due to the large instantaneous power demand, conventional TMS devices often use LC oscillator circuits, which generate damped cosine stimuli efficiently and without requiring very large power switches, but they can produce only restricted stimulus shape options. The technical limitations of existing methods may limit their clinical effectiveness, and certainly constrain their potential for TMS stimulation in research.

The rapid advance in power electronics technology has made it possible to more precisely control the peak megawatt electrical power required in TMS devices. This control is often used for the generation of near-rectangular pulses. For example, controllable TMS (cTMS) devices were introduced in 2008, 2011 and 2014 with three different architectural variations. These designs generated a near-rectangular stimulus whose pulse width is adjustable [4]–[6]. Pulse amplitude (so-called TMS intensity) setup was performed separately using adjunctive equipment. The use of two different DC supply voltages (in the second and third versions) provides greater flexibility but increases the complexity and cost of the system (for example, when attempting energy rebalancing between the capacitors in the monophasic repetitive protocols). In addition, because the system is not symmetric, the

Manuscript received May 22, 2020; revised July 14, 2020 and September 6, 2020; accepted September 6, 2020. Date of publication September 18, 2020; date of current version May 20, 2021. This work was supported by a programme grant from the MRC Brain Network Dynamics Unit at Oxford, as well as supplemental funding to Denison by the Royal Academy of Engineering and Wendt by an MRC iCASE fellowship. *(Corresponding author: Majid Memarian Sorkhabi.)*

Majid Memarian Sorkhabi is with the MRC Brain Network Dynamics Unit, University of Oxford, Oxford OX1 3TH, U.K. (e-mail: majid.memariansorkhabi@pharm.ox.ac.uk).

Moaad Benjaber, Karen Wendt, and Timothy O. West are with the MRC Brain Network Dynamics Unit, University of Oxford.

Daniel J. Rogers is with the Department of Engineering Science, University of Oxford.

Timothy Denison is with the MRC Brain Network Dynamics Unit, University of Oxford and also with the Department of Engineering Science, University of Oxford.

Digital Object Identifier 10.1109/TBME.2020.3024902

stimulus polarity can only be reversed by mechanically changing the orientation or connection of the stimulation coil.

To improve TMS flexibility, flexTMS was introduced by Gattinger *et al.* in 2012 [7]. This instrument uses a single external DC source and employed a H-bridge structure to control resonance at different time intervals. Several limitations of flexTMS result from its small energy storage capacitors, which cause a large voltage decay at the beginning and end of each pulse, and greatly reduce the effective pulse width. The flexTMS design is optimized for producing pulses up to 200 μs wide. In addition, relatively large-amplitude oscillation artifacts are seen in the switching sequence. Other designs have demonstrated more adjustable stimulus parameters, although they are generally restricted to low power and thus are only suitable for small-animal experiments [8], [9].

Implemented TMS architecture uses standard power-electronic modulation techniques with a non-resonant, high-frequency switching architecture to construct arbitrary, high-power waveforms. Specifically, we employ pulse width modulation (PWM) to drive a H-bridge circuit in order to create a highly controllable AC output waveform from a DC source. PWM is a common technique used extensively in electric motor drivers, solar photovoltaic (PV) inverters and a multitude of other power conversion applications [10], [11]. PWM provides the ability to synthesize an AC output stimulus pulse with variable frequency and amplitude from a single DC input voltage source. The fundamental principle of PWM for TMS is to supply a sequence of constant-amplitude, variable-width pulses of DC voltage to the coil to approximate the desired stimulus. The shape and the average value of the stimulus across the stimulation coil are managed by sequentially switching semiconductor switches on and off.

PWM produces sharp-edged rectangular voltage pulses that have significant high frequency content. This should, ideally, be removed by suitable filtering in order to produce the desired TMS stimulus waveform. In a TMS application, there are effectively two cascaded low-pass filters naturally present in the system: Firstly, the inductance of the stimulation coil provides filtering through integration of the applied PWM voltage leading to the resulting coil current. Secondly, the neural activation response is also low-pass in nature and further reduces the effect of remaining high frequency content in the magnetic field produced by the coil current. To better characterize filter properties of the neural circuit, the effect of a TMS stimulus on a neuronal membrane in the human cortex can be modelled using the leaky integrate-and-fire model. Considering only the subthreshold dynamics, this model describes a cell membrane as a capacitor, which is charged by an incoming current, and a resistor, representing the current slowly leaking across the membrane [12]. The net effect is that the cellular dynamics act approximately as a low-pass filter. When an electric field waveform E(t) is applied to the neuron, the change in membrane potential (ΔV_m) in a specific spatial coordinate is proportional to:

$$\Delta V_m \sim \alpha . E\left(t\right) * h\left(t\right) \tag{1}$$

where '$*$' denotes the temporal convolution, *h(t)* is the impulse response of a low-pass filter [13] and α is a constant value depending on the neural type, length, and location of the neuron relative to the electric field [14]. The impulse response can be defined as

$$h\left(t\right) = \frac{1}{\tau_m} e^{-t/\tau_m}\, u\left(t\right) \tag{2}$$

where u(t) is the Heaviside step function and τ_m is the membrane time constant [13]. Assuming that the transcranial stimulation preferentially stimulates the axons, this time constant is approximately 150 μs [4], [13], [15]. Note that for cellular excitation, the time constant is an order of magnitude larger and so the signal is filtered more strongly; axonal excitation can therefore be viewed as a worst-case scenario for filtering.

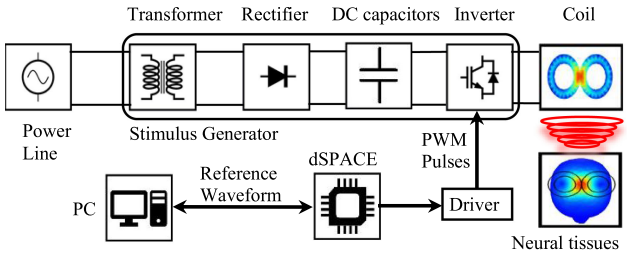

Fig. 1. The overall diagram of the implemented pTMS system.

II. pTMS Design

A. Circuit Topology and Switch Selection

The conceptual block diagram of the implemented programmable TMS (pTMS) system is shown in Fig. 1. The design converts the mains power to high-power magnetic pulses in three distinct stages. The first stage is the step-up of the mains voltage by the transformer. In the second stage, the full-wave rectifier-bridge converts the AC to a DC voltage and contains an energy storage reservoir in the form of DC capacitors. In the third stage, a 3-level H-bridge inverter creates the PWM stimulus from the DC voltage with a non-resonant, high frequency switching design. The dSPACE controller converts the reference waveform generated by the stimulus controller into a train of PWM pulses that operate the switches in the H-bridge. The voltage generated by the H-bridge causes a current to flow in the TMS coil to produce a time-varying magnetic field. According to the Faraday–Henry law, current flows in a conductor (including the nervous tissues) exposed to a time-varying magnetic field. This electrical current leads to the activation of neurons and ultimately causes the excitation/inhibition of central or peripheral nerves.

The H-bridge circuit and control block are illustrated in Fig. 2(a)-(b). This block converts and controls the electromagnetic energy flow between the DC capacitors and the stimulation coil. The transistors in the H-bridge operate as switches, either in the fully-conducting state (near-zero resistance, ON) or fully-blocking state (near-infinite resistance, OFF) states. The OFF-ON and ON-OFF transitions occur very rapidly and so the transistors spend negligible time in a state of partial conduction.

The switches used to construct the H-bridge can, in principle, be any fully-controllable device such as BJTs, MOSFETs, IGBTs, or GTOs (thyristors are not suitable because they cannot

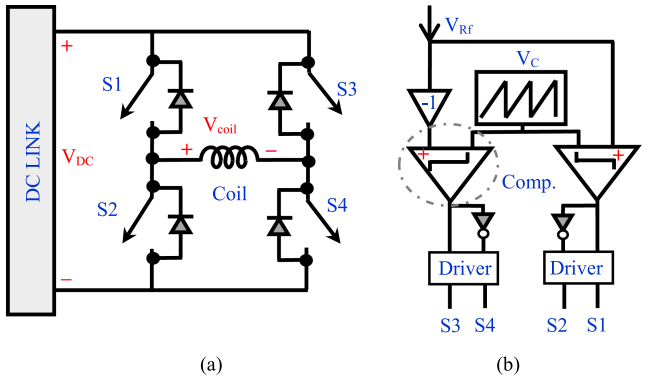

Fig. 2. Basic units for the H-bridge inverter; (a) Power circuit (b) Unipolar PWM logic block to generate the control signal.

be gated off). The silicon IGBT is generally considered to be the most cost-effective selection for medium- to high-power applications operating in the 1–4 kV range with switching frequencies below 20 kHz [16]. Therefore, the IGBT was selected as the power switch in the pTMS system.

B. Operational Principles

The behaviour of the H-bridge inverter for an inductive stimulation coil is illustrated in Fig. 3. The inverter operates in the powering mode, zero mode, and regeneration mode [17], depending on the state of the IGBTs and the direction of the coil current. The details of the paths between the switches, diodes and coil current are outlined in Fig 3(a-h).

In the powering mode, energy is transferred as current from the power line to the coil generating a magnetic field (the magnitude of the coil current increases). In this case, the energy is transferred from the DC capacitors to the coil (modes I and V). In the regeneration mode, the stored energy in the coil field is transferred back to the DC capacitor (magnitude of the coil current decreases, modes IV and VIII). Regeneration represents a recovery of energy and therefore results in a lower average power draw from the mains supply compared to a system that reduces coil current by dissipating energy. In the zero-operation mode, the connection between the coil and the DC capacitors is cut off and the coil is shorted via IGBTs/diodes, so approximately zero voltage is applied to the coil, and the current remains constant (modes II, III, VI, VII). In practice, the intrinsic resistances of the coil and H-bridge transistors result in a small loss in all modes, which will cause heating in these components.

The desired coil current waveform can be produced by controlling the state of the switches in the H-bridge using PWM [18], [19]. To derive switching states for each switch in the H-bridge, a common method is to compare the reference signal ($+\mathrm{V_{Rf}}$) with a carrier signal ($\mathrm{V_C}$), as demonstrated in Fig. 2(b). Generally, the carrier signal is a triangular waveform and its frequency is several times that of the reference signal frequency, where the reference signal is the requested stimulus waveform to be mimicked by the PWM. In order to generate a three-level output the carrier signal is compared with two reference signals, which are of the same magnitude and frequency but 180 degrees out of phase ($\mathrm{V_{Rf}}$ and $-\mathrm{V_{Rf}}$). This method is called unipolar PWM (UPWM) with two phase-shifted reference signals [20].

An example of this process for a simple cosine reference signal is shown in Fig. 4. According to Fig. 2(b) and Fig. 4, ($+\mathrm{V_{RF}}$) and ($-\mathrm{V_{RF}}$) are used for controlling (S1-S2), and (S3-S4) respectively. As can be observed from Fig. 4, each switch is operated several times in one cycle of the reference signal. In this switching scheme the stimulus voltage level changes between either 0 and $+\mathrm{V_{DC}}$ or from 0 and $-\mathrm{V_{DC}}$; the stimulus has three discrete levels: 0, $-\mathrm{V_{DC}}$, and $+\mathrm{V_{DC}}$.

One of the major advantages of the PWM approach to TMS systems is the ability to adjust the stimulus power by changing the reference wave amplitude, meaning that the stimulus intensity can be adjusted rapidly without needing to vary the DC voltage produced by the rectifier. If the maximum value of the reference is equal to the maximum value of the triangle carrier, the H-bridge will generate the highest voltage. In the PWM technique, the amplitude modulation index ($\mathrm{m_a}$) is [21]:

$$m_a = \frac{\widehat{V_{Rf}}}{\widehat{V_C}} \tag{3}$$

where $\widehat{V_{Rf}}$ and $\widehat{V_C}$ are the peak values of the reference and carrier signals, respectively. $\mathrm{m_a}$ is commonly adjusted by varying the peak of V_{Rf} while keeping V_C constant. The H-bridge inverter can generate an output voltage linearly proportional to the reference wave in the range of $0 \leq m_a \leq 1$ [16]. The frequency modulation index (m_f) is determined as [21]:

$$m_f = \frac{f_C}{f_{Rf}} \tag{4}$$

where f_C and f_{Rf} are the frequencies of the carrier and reference signals, respectively. Clearly, whilst the voltage output generated by the H-bridge contains the desired fundamental component, it is also rich in high frequency harmonics. In unipolar PWM, the first set of harmonics are the largest and are distributed around $2\mathrm{f_C}$ [21], and then occur at higher multiples of $\mathrm{f_C}$. By increasing the frequency modulation index (by increasing the carrier frequency), the undesirable higher harmonics can be moved away from the fundamental, which will improve the low-pass filtering effect of the stimulus coil and nervous system and so provide a higher-fidelity response. However, $\mathrm{f_C}$ is limited by the capability of the H-bridge switches – increasing $\mathrm{f_C}$ will tend to increase losses and will eventually lead to overheating.

In the TMS system, the coil connected to the pulse generator is inductive, so the inverter circuit must always have an alternate path to allow the coil current to continue to flow when the switch is turned off. For this purpose, an antiparallel diode must be connected across each power switch, as shown in Fig. 2(a).

C. Physiological Response Models for the PWM Stimulus

A key assumption is that the neural substrate will act as a low pass filter to suppress the high frequency content of the PWM stimulus. Barker et al. estimated the time constant of the nerve membrane under electromagnetic stimulation to be in the order of 150 μs [15]. In prior work characterizing TMS systems, the same time constant has been used to predict changes of axonal

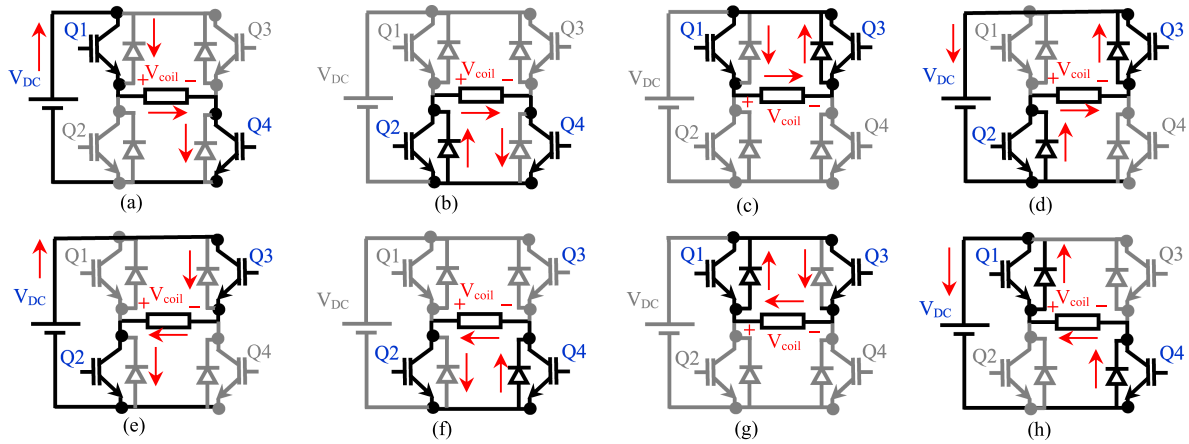

Fig. 3. Equivalent circuits of the 3-level inverter in the different operating modes when connected to the inductance load of the stimulation coil; (a) Mode (I); (b) Mode (II); (c) Mode (III); (d) Mode (IV); (e) Mode (V); (f) Mode (VI); (g) Mode (VII); (h) Mode (VIII).

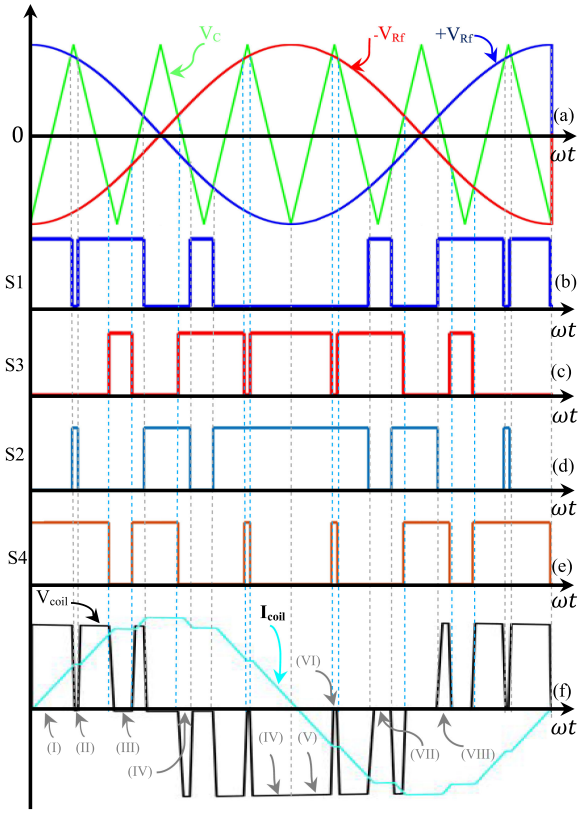

Fig. 4. Basic key waveforms of the UPWM H-bridge inverter ($f_{Rf} = 2.5$ kHz, and $f_c = 15$ kHz, $m_f = 6$, $m_a = 0.9$). (a) Triangular waveform comparison with 2.5 kHz cosine reference (V_{Rf}) and 180° shifted reference ($-V_{Rf}$). (b) Trigger signal for S1. (c) Trigger signal for S2. (d) Trigger signal for S3. (e) Trigger signal for S4. (f) Coil voltage and current and working modes (I-VIII).

membrane potential in response to stimulation [4]. To allow comparisons of the performance of the implemented system and other studies, a similar value is considered to determine nerve membrane dynamics. By connecting a passive RC filter (R represents membrane resistance and C represents membrane capacitance) with a combined time constant of 150 μs, the output

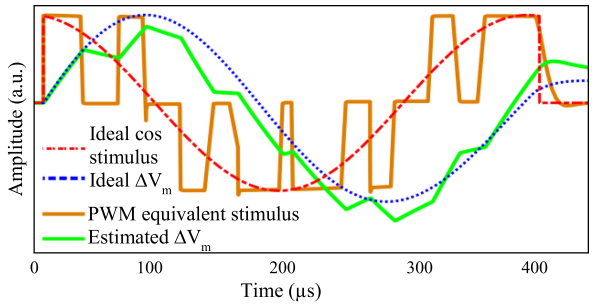

Fig. 5. Simulation of the ideal and approximated behavior of a neuronal membrane during transcranial stimulation, together with the applied pulse-width modulated coil voltage.

of the filter can be considered as an estimate of the changes in membrane potential (ΔV_m) [22].

The approximation of the membrane as a low-pass filter supports the principle of using PWM in our design. To illustrate this, Fig. 5 shows the membrane voltage change (ΔV_m) for a 2.5 kHz cosine stimulus as generated by the PWM method compared to an ideal waveshape (this shape can be induced by the Magstim Rapid system).

Membrane voltage changes for the ideal pulse are consistent with the experimental results of the measurements presented in [22]. For the PWM stimulation, although some slight residual distortion due to high-order harmonics generated by the PWM process is visible, the membrane potential change closely follows the shape of the ideal sine wave, validating the use of the pulse-width modulated coil voltage.

Using the introduced physiological model, it is also possible to estimate neural behavior in the suprathreshold stimulation and the spike firing of the neuron by defining and selecting a certain threshold value [12].

III. Circuit Design Details

We constructed a prototype to demonstrate the design concepts. The prototype was a complete circuit cross-section intended for design evaluation with existing coil hardware,

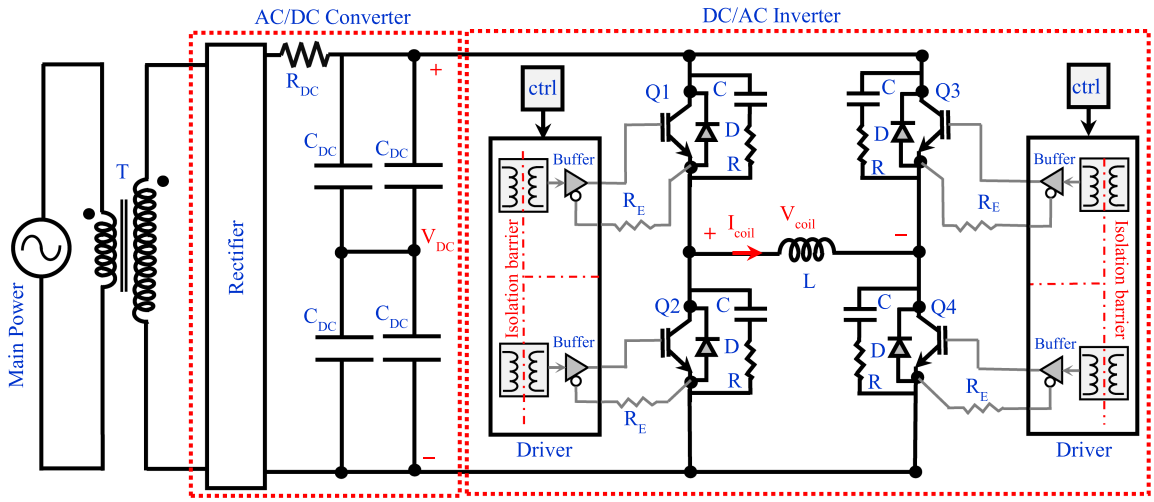

Fig. 6. Detailed schematic of the pTMS power circuitry. The black lines indicate high-voltage high-current connections and the grey lines indicate low-voltage low-current control lines.

TABLE I
KEY COMPONENTS OF THE PTMS

Component	*Assignment*	*Nominal Rating*	*Part Number*	*Manufacturer*
T	Step-up transformer	Output: 1 kV,10 A Class-E insulation	Custom manufactured	Eastern Transformers, UK
Rectifier	Full bridge diode rectifier	1200 V, Ultrafast recovery diode I_{FRM} [a] = 600 A	STTH9012TV1	STMicroelectronics
R_{DC}	Charging resistor	2x 47 Ω, thick- film on steel 2.5 kV, 1.5 kW (parallel)	WDBR1-47RKT	TT ELECTRONICS
C_{DC}	Energy storage	10000 µF, 500 VDC Aluminum capacitor	ALS70A103NT500	KEMET Electronics
Q1-Q4	IGBT power switch	1.2 kV I_{CRM} [b] = 1.8 kA Q_G = 3.45 µC	SEMiX603GB12E4p	Semikron
D	Free-wheeling diode (included in the IGBT module)	1.2 kV I_{FRM} [c] = 1.8 kA		
C	Snubber capacitor	2 µF, Polypropylene film capacitor	205PPA122K	Illinois Capacitor
R	Snubber resistor	1Ω, non-Inductive film resistor	AP821 1R F	Arcol
Scale 2+ driver core	Gate driver core	VGE_{on}= 15 V, VGE_{off}= -8 V, I_G = 6A.	2SC0106T2A1-12	Power Integrations
R_E	Emitter resistor	500 mΩ,	AP821 R5 J	Arcol
L	Stimulation coil	15.5 µH	D70 Remote Coil	Magstim
ctrl	Digital controller	PWM generation resolution: 10 ns	MicroLabBox, includes Power PC Dual Core 2 GHz processor, DS1202, DS1302 I/O	dSPACE

a) Repetitive peak forward current, tp = 5 μs, F= 5 kHz square. b) Peak current value at collector output during pulse operation. C) Repetitive peak forward current of the free-wheeling diode.

and not scaled for immediate clinical translation. The detailed structure of the implemented pTMS is demonstrated in Fig. 6, and the main components used in the implementation of pTMS are provided in Table I.

A. Rectifier and DC Capacitor

The rectifier and DC capacitor condition energy from the mains for the H-bridge. Referring to Fig. 6, the AC/DC converter comprises a full-wave diode rectifier, a current limiting resistor, and four high-voltage energy-storage capacitors. The size of the DC capacitors determines the maximum energy that can be delivered in one pulse. The DC link voltage change ΔV_{DC} after the stimulus delivery (valid for small $\frac{\Delta V_{DC}}{V_{DC}}$), can be calculated as

$$\Delta V_{DC} \approx \frac{1}{V_{\mathrm{DC}} C_{\mathrm{DC}}} \left(P_{\mathrm{supply}} t_{\mathrm{pulse}} - E_{\mathrm{pulse}}\right) \qquad (5)$$

where V_{DC} is the DC link voltage, C_{DC} is the total DC link capacitance, P_{supply} is the average supply power, t_{pulse} is the pulse duration and E_{pulse} is energy per pulse in Joules. The DC capacitor should be sized to give no more than a 5-10% voltage drop for the worst-case pulse, otherwise stimulus waveform quality may be adversely affected. For brief

pulses ($t_{pulse} << \pi\sqrt{L_{coil}C_{DC}}/2$), the capacitor voltage can be assumed to be almost constant. Repetitive-pulse protocols, such as theta-burst stimulation (TBS) [2] will tend to drive the determination of the capacitance value because they represent a high average power. The current limiting resistor (R_{DC}) restricts the peak current of the capacitor during the charging cycle. In the repetitive protocols, proper heatsinking of these resistors is required due to the high rate of pulses drawing significant power from the mains.

B. H-Bridge Implementation Details

TMS requires the generation of very high peak power pulses (over 3 MW), which will typically exceed the switching capability of individual IGBT die. However, the average power of TMS is relatively low (a few hundred Watts in repetitive modalities). Therefore, TMS is an example of a pulsed power application which tend to place severe electrical and thermal stresses on the transistors [23], [24]. Due to the importance of repeatability and stability in medical devices, as well as operator and patient safety, all components of the TMS should be strictly operated in their safe operating area (SOA) to ensure reliability.

The parallel connection of IGBT dies is necessary for increasing the current carrying capacity of transistors beyond that of a single die [25]. In our implementation of pTMS, two parallel IGBT modules are used in each leg (totalling 4 modules for the DC/AC inverter block). All eight switches (Q/D) are implemented with 1200V/1800A IGBT modules (Semikron, Germany). The tolerances in IGBT parameters, process variations, unbalanced stray inductance in the circuit, and dissimilar propagation delays in driver circuits can cause asymmetrical current sharing among parallel-connected IGBTs under both static and dynamic operation [25]. In our implementation, IGBT emitter resistors (R_E) are used to encourage current sharing between the parallel-connected modules, as shown in Fig. 6.

The IGBT module baseplate temperature is measured continuously using the NTC thermistor embedded in the module. A real-time temperature measurement is used by the dSPACE controller to shut down the system and halt operation if outside a prescribed limit.

C. IGBT Gate Driver

The gate driver circuit provides the transient currents required to charge/ discharge the MOS-gate structure of the IGBTs. During the switching transient, the driver can also control the dv/dt and di/dt rate by the external $R_{G(off)}$ and the $R_{G(on)}$, respectively [26]. Controlling the transient behaviour of the circuit helps to reduce the stress on switches.

To drive the parallel-connected switches in each leg, a central driver with separate external resistors is used. As well as emitter resistors, symmetrical wiring between driver and IGBTs, DC link and inverter, and inverter and stimulation coil helps to further encourage current sharing. In the experimental setup, current imbalance between switches was observed to stay below 5% during all phases of operation.

D. Snubber Circuit

The stray inductance of the commutation path can cause large over-voltages in the switches at turn-on and turn-off. By minimizing the lengths of interconnecting busbars, this inductance may be reduced but never completely removed (for example, there is always some internal stray inductance associated with the IGBT bond wires and package leads). The highest overvoltage generally occurs during switch-off due to the reverse recovery effect of the opposing diode. This transient voltage could exceed the maximum blocking voltage of the power switches and can destroy the IGBT [27].

Snubbers offer protection against voltage transients during the turn-off switching and maintain the IGBT in the SOA [28]. In the implemented pTMS structure, each IGBT switch is protected by a passive RC snubber network (Table I). A penalty is that snubbers (and larger gate resistors) will tend to increase turn-off time and therefore increase switching loss.

E. System Controller

The pTMS system is controlled and monitored by a MicroLabBox commercial control system (dSPACE GmbH, Germany). The generation of high-resolution (10 ns) PWM trigger pulses enables the precise generation of stimulus pulses. The controller output parameters include four PWM signals to trigger the IGBTs, according to the logic block mentioned in Fig. 2(b). The input parameters of the controller include the reading of the IGBT module temperatures, the voltage of the stimulation coil and the stimulation current in the coil.

If any of these input parameters exceed the predefined values during the experiment, the stimulation process stops, which helps ensure that the TMS components are kept within their SOA.

IV. Experimental Results

A. Stimulus Voltage, Current Shape, Induced Electric Field and Membrane Dynamics

The stimulus voltage and current values of the circuit are dependent on the inductance of the coil (arising from the electromagnetic design of the particular coil), the frequency of the stimulation, and the amplitude modulation index. Representative measurement results of the pTMS system are shown in Fig. 7(a-d). The pTMS was tested with a link voltage of VDC = 1000 V and peak coil current up to 3600 A. The maximum energy transferred to the D70 Remote coil (Magstim, UK) was 100.4 Joules. The coil voltage and current were measured via a high- voltage differential probe (TA044, PICO TECHNOLOGY, UK) and a Rogowski current probe (I6000S FLEX-24, FLUKE, USA), respectively. All measurements were performed with a digital oscilloscope and a sampling rate of 250 MSa/s. No bandwidth restrictions or filters have been applied to remove switching spikes. The measurements were performed for two square pulses with widths of 40 and 110 microseconds, a 2.5 kHz cosine pulse with $m_a = 1$, and a 2.5 kHz sinusoidal pulse with $m_a = 0.5$. Modulation indexes are selected to achieve maximum

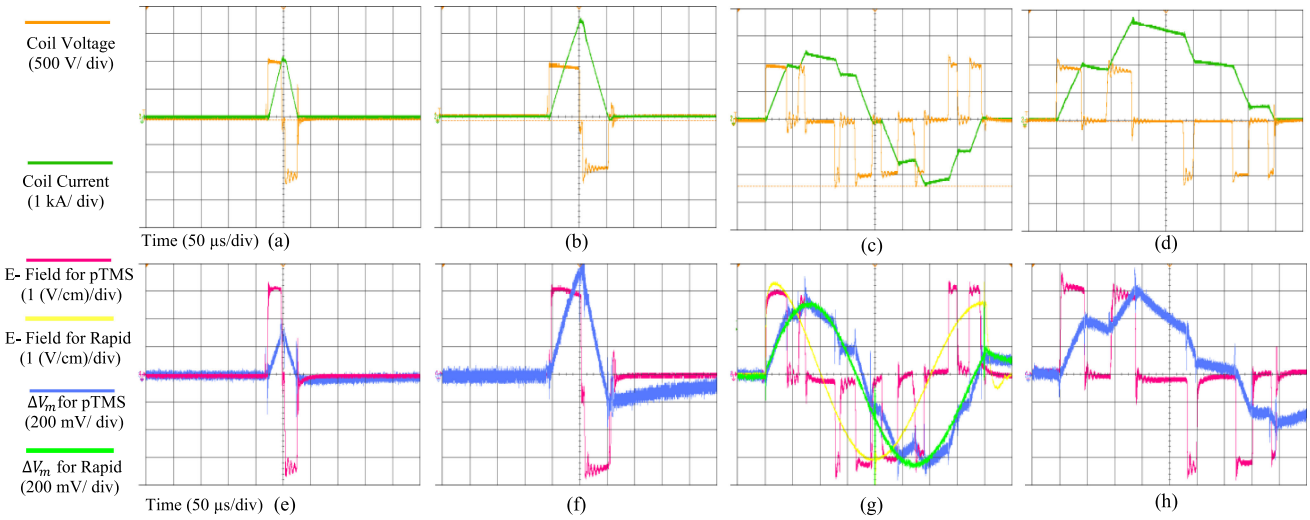

Fig. 7. Measured waveforms for 4 different pTMS stimuli: Voltage and current for (a) 40 μs square stimulus (monophasic output) (20 μs positive and 20 μs negative phase) - (b) 110 μs square stimulus (monophasic output) (55 μs positive and 55 μs negative phase)- (c) 2.5 kHz Cosine stimulus (m_a= 1) (biphasic output)- (d) 2.5 kHz Sine stimulus (m_a= 0.5) (monophasic output). Electric field and neural membrane dynamic for (e) 40 μs square stimulus- (f) 110 μs square stimulus- (g) 2.5 kHz Cosine stimulus (m_a=1) and Magstim Rapid^2 system measures- (h) 2.5 kHz Sine stimulus (m_a= 0.5).

output voltage/current value, as well as ensuring that the circuit operates in the SOA.

The induced electric field (E) was measured with a custom-made pickup coil consisting of a single-turn rectangular winding (0.15-mm-thick copper wire). The pick-up coil dimensions were 1 cm $\times$ 35 cm, in a perpendicular position to the stimulation coil center. The small side of the rectangular pick-up coil was located 1 mm away from the surface of the coil. The value of the induced electric field can be estimated by dividing the measured electromotive force (EMF) by the search coil width (w), as (6).

$$E \cong EMF/w \tag{6}$$

If the search coil width is 1 centimeter (w = 1 cm), the measured EMF is approximately equal to the induced electric field (E) measured in V/cm [29], [30]. To estimate the behavior of the nerves stimulated by the induced electric fields, a physiological model should be considered, as mentioned in Section (II-C).

The experimental results of the induced electric field and the predicted membrane potential corresponding to the first-line stimuli along with measures for the Magstim Rapid system, are shown in Fig. 7(e- h). The induced electric field waveform follows the stimulus waveform, and the shape of the estimated change in membrane potential is similar to the stimulus current waveform (except the phase difference in I_{coil} and ΔV_m caused by charging/ discharging capacitors). The measurement results prove that the briefer pTMS pulses will induce smaller changes in membrane potential, and the longer pulses that have more energy will produce larger ΔV_m. These results are consistent with a prior study [31].To ensure that the induction electric field generated by pTMS was sufficient for the nerve stimulation, some measurements were repeated on the Magstim Rapid^2 option 2 device (Magstim Company Ltd, UK). The experimental results confirmed that the maximum induction electric field of the pTMS device is 63% of the maximum of the Magstim Rapid^2. While some references report that the average motor evoked potential (MEP) is 40.6–55% of the maximum power of some commercial TMS devices [32]–[34], this parameter also depends on the TMS stimulus generator, stimulation coil, gender and age of the individual [34].

The motor threshold value may also be changed by adjusting the stimulus frequency (or pulse width) [6], [31], [35]. In cases where the maximum output intensity at high frequencies does not reach the motor threshold, pulses with lower frequencies can be used. The same stimulus parameters can be used for an intervention session. The impact of this power limitation is limited to single pulse, low duty cycle experiments. For higher pulse rates, the programmable TMS achieves parity with the Magstim Rapid^2, as discussed in the next sections.

B. Safety, Commutation Performance, Relative Heating

The oscillations visible in the voltage and electric field are due to the action of the snubber circuit to compensate for transient voltages created during switch commutation. These transient oscillations are caused by stray inductors in the circuit and IGBTs, as discussed in Section III. For transient voltage spikes, a 20% safety margin was achieved.

Experimental measurements confirmed that the driver and the snubber circuit were able to keep the IGBTs within their SOA throughout operation. Furthermore, Fig. 7(a-d) demonstrates the pTMS stimuli have almost the same pulse amplitude at the beginning and end of the voltage pulse due to the large DC capacitor. As shown in Fig. 7(b), after a pulse of 55 μs, the voltage drop is approximately 10%.

Experiments prove that the implemented system can generate a wide range of stimulus waveforms. The operator defines the desired waveform as a reference signal, and then the dSPACE

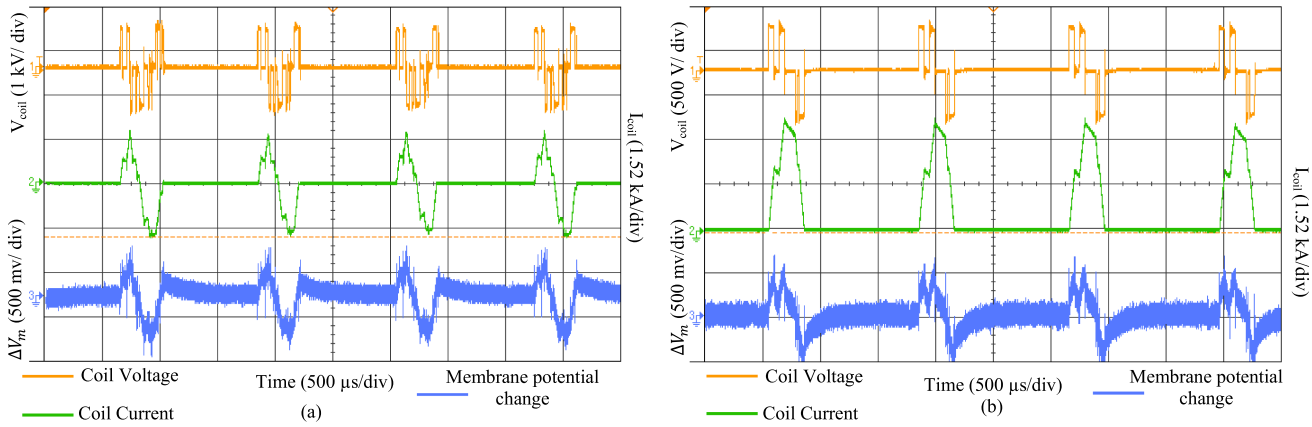

Fig. 8. Waveform parameters measured for four cosine and four sine stimuli, as QPS modality- (a) Cosine pulse with 800 μs interstimulus interval, as a biphasic stimulation. - (b) Sine pulse with 1000 μs interstimulus interval, as a monophasic stimulation. For these measurements, the oscilloscope sampling rate was 100 MSa/ s.

calculates the PWM signal required to drive the TMS coil appropriately.

To characterize the effect of the PWM stimulus on coil heating, an experiment was conducted on the D70 remote coil (Magstim Company Ltd, UK). The stimulation pattern was chosen as iTBS (triplet 50 Hz bursts, repeated at 5 Hz; 2 seconds on and 8 seconds off; a total of 180 pulses) and the temperature of the coil center was measured with a thermal camera (FLIR C2, FLIR Systems, USA). The experiment was repeated with the Magstim Rapid^2 option 2 device (Magstim Company Ltd, UK). To produce 50 Hz pulses, the maximum output power of Magstim Rapid^2 is limited to 50%. Therefore, the output power of the pTMS was set to the same power ($m_a = 0.8$). The generated waveform was also set as a cosine of 2.5 kHz ($m_f = 6$). The experiment was performed at the same ambient temperature and the coil temperature was measured at the beginning and end of the iTBS. No significant temperature difference was observed.

C. rTMS and Arbitrary Stimulus Sequence Generation

rTMS has become a major area of TMS research in the last decade. This technique has been studied as a novel paradigm in treatment in a variety of neurological and psychiatric disorders [36], [37] and motivates new pulse shapes and patterns. Short inter-stimulus intervals are conventionally generated by connecting multiple devices to a single coil.

For example, to produce a train of four monophasic magnetic pulses with a time interval of 1.5–1250 ms (called Quadri-pulse stimulation: QPS), four Magstim TMS devices are connected with a specially designed combining module [38], [39]. Eliminating these costly solutions motivates the design of new circuits for the generation of magnetic stimuli that can provide the ability to generate consecutive pulses required for novel therapies and experiments. In therapies invoking rTMS, the time interval between pulses is typically short, but the AC/DC power converter circuits from the mains are not capable of rapidly charging capacitors. Therefore, the designed circuits must be able to recycle the energy supplied to the coil, as discussed in Section (II-B). In our design, the high capacitance in the AC/DC converter allows the DC link voltage to remain constant during the short pulses.

Fig. 8 illustrates an example of the pTMS system's capability in generating repetitive pulses, while recovering energy from the TMS coil. The measured parameters were set up for the generation of four cosine and four sinusoidal stimuli with an interstimulus interval of 800 μs and 1000 μs, respectively. After four pulses, the DC link voltage drop caused by the losses in the circuit was 1%. With a very short time interval, a consistent stimulus can be generated and a stable potential change in the membrane can occur. Using the QPS protocol [39], the proposed system can generate 360 monophasic stimuli in 30 minutes, without a coil heating issue (coil temperature less than 40 °C).

The performance of the PTMS system in the iTBS and cTBS modalities was also evaluated. In this technique, three pulses repeated with an interstimulus interval of 20 milliseconds (50 Hz burst of the 3 stimuli) based on the protocol defined in [2]. The measured parameters are similar to Fig. 8. The losses occurring in the long interstimulus interval (caused by the parasitic coil path resistance) are compensated by the recharge of the DC link from the mains supply.

A key feature of the pTMS system is the ability *to maintain power in high repetition rate protocols*. In commercial devices such as the Magstim Super Rapid^2 Plus, the maximum stimulator output decreases with increasing repetition rate; for example, for a 10 ms inter-pulse interval (equivalent to a 100 Hz repetition rate) the MSO drops to 49%. In contrast, the implemented magnetic neurostimulator can generate and deliver 63% MSO, even at pulse intervals of 1 ms (equivalent to a 1000 Hz repetition rate).

We note here that the protype system in this paper is intended to be a demonstrator of the technology, and not a production-ready design; it uses the minimum number or parallel modules (i.e. 2) to demonstrate viability and potential scalability of the circuit. We predict that if the number of parallel IGBTs were to be increased to three, the MSO would increase to 88% and four would allow an MSO of 100%, as per Fig. 9. As the number of parallel IGBTs is increased, the coil should be modified such

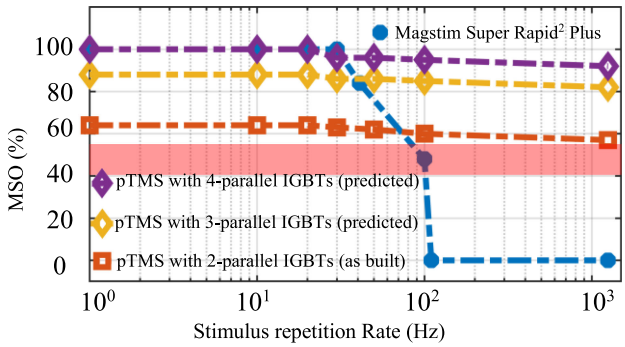

Fig. 9. Comparison of the maximum stimulator output (MSO) values of the pTMS system and the Magstim Super Rapid^2 Plus device. The red shading depicts the average MT for the single TMS pulse in human experiments [32]–[34].

that its inductance is decreased proportionally. This ensures that the rate-of-rise of current is increased in proportion to circuit delivery capability, i.e. that larger magnitude current waveforms can be delivered at the same bandwidth. In most cases this would simply require a rewinding of the coil with a reduced number of turns constructed of correspondingly thicker conductors.

V. Discussion

The characteristic ability of TMS to provide non-invasive brain stimulation, coupled with the large unmet need of deriving better treatments for neurological disorders, motivates the development of improved capabilities of TMS systems to deliver more flexible patterns of stimulation.

Most current research in this field focuses on the number of pulses per second, the time interval between pulses and sessions [40]. However, the introduction of new devices that can produce stimuli in a wide range of flexible patterns could open new pathways for clinical neuroscience. This research has presented a new TMS device that generates highly flexible stimulus waveforms in terms of both pulse shapes as well as patterns. To achieve this performance, the unipolar PWM technique and the application of 3-level H-bridge inverters in the TMS stimulus generator were explored. Consistent with the PWM principle, the generation of pulse trains of different widths and polarities allowed the imitation of a wide range of pulses (although with the trade-off of increased harmonic distortion in some cases).

A. Comparison to the State-of-the-Art

To compare the results of this study with the state-of-the-art, recent important published papers in the field of generating controllable stimuli are summarized in Table II. The purpose of this table is to compare the architecture of circuits, stimuli

waveforms generated by different systems and their key parameters. The circuit structures with the parameters presented in their respective papers were simulated in MATLAB Simulink software (Powergui blockset). The D70 remote coil (Magstim Company Ltd, UK) with a 15.5 μH inductance and a 20 mΩ parasitic resistance is selected for all structures. The total stray inductors in the circuits and IGBT equivalent on-resistance $R_{CE\ (on)}$ are considered to be 20 nH and 1.5 mΩ, respectively. Necessary changes have been made in the snubber circuits to optimize the overshoot-undershoot and voltage spikes resulting from the new circuit conditions.

The TMS circuits are divided into two main categories: resonant and switching architectures. The stimulus waveform produced by a resonant circuit depends on the coil inductance, the capacitance of the pulse capacitor, and the initial pulse capacitor voltage. Switching circuits generate near-rectangular pulses, and the stimulus waveform is determined by the switching pattern of the power switches. Circuits that are switched at low frequencies can only generate limited pulse shapes, but circuits that are switched at high frequencies are able to mimic arbitrary stimuli.

The DC link voltage, the coil voltage and current waveforms generated by these structures are presented in the third column of Table II. The key features of the stimulus and the circuit parameters are given in columns 4 and 5, respectively. For each structure, the total energy storage capacitors (C_{ES}) and the maximum DC link voltage ($V_{DC\ link}$) are shown in the table and provide an overview of the AC/DC converters. The maximum pulse widths of each structure were calculated according to the topics discussed in Section (III-A) and are given in the fourth column of the table. We summarize the key architectural innovations in the table here.

1) The flexTMS was introduced to control LC resonance at different time intervals [7]. Although the flexTMS circuit is superficially similar to an H-bridge, as the pulse capacitor is used in resonance with the coil the stimulus waveform depends strongly on the circuit parameters. As seen in Table II, by using three voltage levels, the architecture can generate near-sinusoidal pulses. The characteristic time of this pulse is one-quarter of the DC capacitance-coil inductance resonance period ($T = \pi\sqrt{LC_{DC}}/2$). For shorter pulses, the voltage across the DC capacitor will fall as energy is transferred to the coil.

By selecting small energy storage capacitors in the flexTMS device, a large voltage drop occurs during each pulse, even though the output waveform is sinusoidal, as evident in Table II. Therefore, limited pulse widths can be generated with a given set of hardware (coil, capacitor); otherwise the hardware must be switched in and out. No specific measurements for Flex-TMS system performance in stimulus voltage decay have been performed in repetitive modalities in [7].

In addition, quite small capacitors increase the sensitivity of the Flex-TMS to a change in the coil inductance since the shape of the magnetic stimulus is directly dependent on the coil inductance and pulse capacitor capacitance. The width of the generated pulse can be changed according to the switching rate. No specific algorithm for IGBT switching was introduced and the performance was evaluated using only a predetermined number of pulses. Note that the stimulus polarity direction generated by the Flex-TMS system can be changed by altering the IGBT switching patterns because the circuit is symmetric.

2) Recently, a structure based on an oscillator with a capacitive fast charger circuit was proposed in [41]. The charging circuit first charged two capacitors of 454 μF, then the energy stored in these capacitors was used to

TABLE II
COMPARISON BETWEEN THE IMPLEMENTED pTMS AND OTHER STRUCTURES FOR SET HARDWARE CONFIGURATION

	Ref.	Circuit structure	Stimulus voltage and current shape	Specifications of the stimulus	Specifications of the circuit
Resonant based circuits	Flex TMS [7]	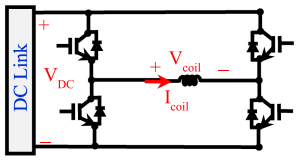	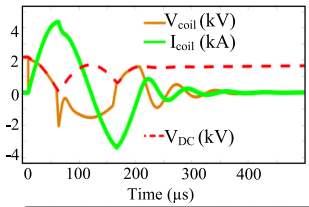	**Shape:** Near sinusoidal monophasic and biphasic **Maximum positive pulse width:**50 µs **Maximum negative pulse width:** 50 µs **Polarity adjustment:** Electrical	$C_{ES\ (DC\ link)} = 66\ \mu F$ $V_{DC\ (max)} = 2.2\ kV$ $I_{coil\ (Max)} = 5\ kA$ $\Delta W_{C_{ES}} = 20.2\ J$
	[41][a]	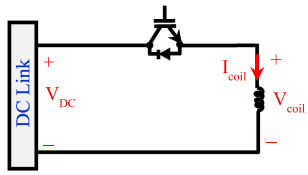	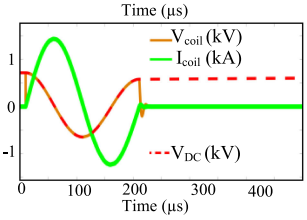	**Shape:** Static cosine shape **Pulse frequency:** 4.97 kHz **Polarity adjustment:** Mechanical[b]	$C_{ES\ (DC\ link)} = 66\ \mu F$ $V_{DC\ (Max)} = 720\ V$ $I_{coil\ (Max)} = 1.66\ kA$ $\Delta W_{C_{ES}} = 10.8\ J$
Switching based circuits	cTMS1 [4]	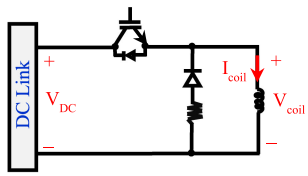	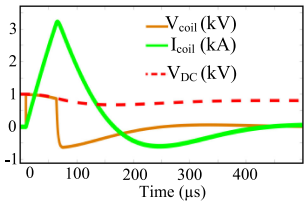	**Shape:** Near rectangular, monophasic **Maximum positive pulse width:**165 µs **Polarity adjustment:** Mechanical[b]	$C_{ES\ (DC\ link)} = 716\ \mu F$ $V_{DC\ (Max)} = 1.65\ kV$ $I_{coil\ (Max)} = 6\ kA$ $\Delta W_{C_{ES}} = 284.5\ J$
	cTMS2 [5]	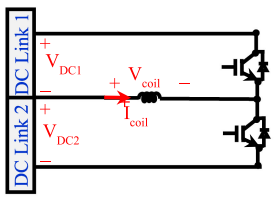	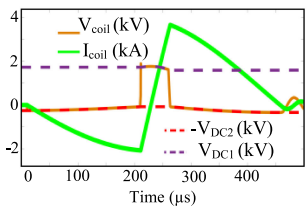	**Shape:** Near rectangular monophasic and biphasic **Maximum positive pulse width:**168 µs **Maximum negative pulse width:** 338 µs **Polarity adjustment:** Mechanical[b] (for the maximum output)	$C_{ES\ (DC\ link1)} = 740\ \mu F$ $C_{ES\ (DC\ link2)} = 3\ mF$ $V_{DC1\ (Max)} = 2.8\ kV$ $V_{DC2\ (Max)} = 1\ kV$ $I_{coil\ (Max)} = 7\ kA$ $\Delta W_{C_{ES}} = 49\ J$
	cTMS3 [6]	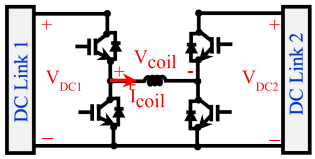	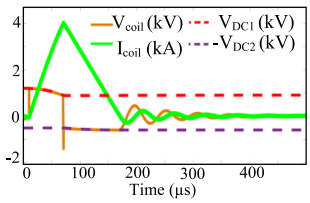	**Shape:** Near rectangular, monophasic and biphasic **Maximum positive pulse width:**128 µs **Maximum negative pulse width:** 276µs **Polarity adjustment:** Mechanical[b] (for the maximum output)	$C_{ES\ (DC\ link1)} = 430\ \mu F$ $C_{ES\ (DC\ link2)} = 2\ mF$ $V_{DC1\ (Max)} = 2.6\ kV$ $V_{DC2\ (Max)} = 1\ kV$ $I_{coil\ (Max)} = 6\ kA$ $\Delta W_{C_{ES}} = 37.6\ J$
	pTMS	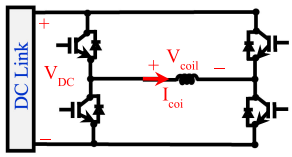	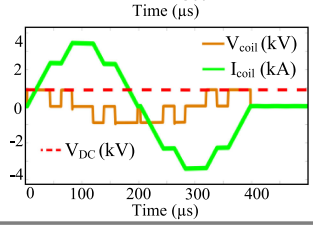	**Shape:** PWM, monophasic and biphasic **Maximum positive pulse width**: 618 µs **Maximum negative pulse width:** 618 µs **Polarity adjustment:** Electrical	$C_{ES\ (DC\ link)} = 10\ mF$ $V_{DC\ (Max)} = 1\ kV$ $I_{coil\ (Max)} = 3.6\ kA$ $\Delta W_{C_{ES}} = 73.1\ J$

a) The circuit parameters corresponding to the qTBS were selected. b) Mechanical change means changing the orientation or connection of the stimulation coil.

rapidly and sequentially charge a 66 μF capacitor. When turning on the IGBT, an oscillation is established between the pre-charged capacitor and the stimulation coil, which can be either interrupted after one period to generate a single biphasic pulse, or left oscillating for several pulses. Pulse shaping is not possible in this structure and the pulse frequency is always constant (determined by the circuit component values). The system was shown to generate four consecutive pulses with an interstimulus interval of 1000 μs.

As shown in Table II, in resonant-based circuits, the coil voltage follows the DC link voltage (red dashed line). Therefore, power switches do not change the stimulus waveform and only determine the pulse time period.

3) To control the pulse width of the stimulus, the idea of replacing the thyristor with an IGBT was proposed by

Peterchev *et al.* in 2008 (controllable TMS1 or cTMS1) [4]. As shown in Table II, the generated stimulus in this system is a single monophasic pulse. The resistive damping used in this circuit has a relatively large power loss. Therefore, it is not possible to produce high-frequency pulse trains and its maximum pulse output rate is one pulse per second. To change the pulse polarity, the orientation of the coil must be changed mechanically (because the circuit is not symmetric with respect to the coil).

4) By using a half-bridge inverter structure, monophasic and biphasic near-rectangular stimuli can be generated (cTMS2) [5]. As demonstrated in Table II, the use of two asymmetric structures in the DC link forces the stimulus to have a positive phase with a higher voltage but lower width and a negative phase with a lower voltage and a higher width. Due to the asymmetric structure of the DC link, the pulse polarity direction cannot be reversed without changing the coil connection direction at 100% MSO.
5) Peterchev *et al.* utilized the H-bridge inverter structure to generate near-rectangular pulses (cTMS3) [6]. Two DC links with different voltages and capacitors were used to generate 4 voltage levels (V_{DC1}, V_{DC2}, V_{DC1}- V_{DC2}, 0), as demonstrated in Table II. The main advantage of this system compared to cTMS2 is the reduction of the voltage stress on the IGBTs by using four IGBTs. However, for any desired rectangular stimulus, a combination of 4 voltage levels and 4 different pulse widths must be prepared (the control algorithm was not fully described in [6]). The IGBTs used in the cTMS3 device are of the 3.3 kV class. For cTMS2, the circuit is not symmetric and so coil connection must be reversed for pulse reversal at 100% MSO.
6) The implemented pTMS system utilises a fully-symmetrical H-Bridge structure, and uses two IGBTs in parallel to increase current rating and reduce current stress on switches. Additionally, the system uses a much larger capacitor in the DC link than other devices and is controlled by the PWM technique instead of operating at the resonant frequency or using a low-frequency on/off switching pattern to generate a single rectangular pulse. However, providing greater control of the stimulus introduces additional switching losses. The utilized IGBTs in the pTMS device are of the 1.2 kV class which can switch at higher frequencies than 3.3 kV class IGBTs due to the associated reduced switching loss per cycle.

To investigate the energy loss of the pTMS device in comparison with that of other structures, as an indicator of energy efficiency, the energy that is not recovered back on the C_{ES} at the end of the stimulus ($\Delta W_{C_{ES}}$) is calculated as in [5]:

$$\Delta W_{C_{ES}} = \frac{1}{2}\left(\sum_{i=1}^{n} C_i V_{C_i}^2\,(\text{start}) - \sum_{i=1}^{n} C_i V_{C_i}^2\,(\text{end})\right) \quad (7)$$

where C_i and n denote energy storage capacitances and the number of them, respectively. Capacitor voltage values (V_{Ci}) are calculated based on MATLAB simulations under the circuit and load conditions described in Section V. A. The energy loss values are shown in Table II. The introduced pTMS device operates at a high switching frequency and so its loss is somewhat higher than others. There is potential to use faster-switching devices (such as silicon-carbide MOSFETs) and/or employ soft-switching techniques to reduce switching losses and increase energy efficiency [42], although at an increase in component cost.

VI. Conclusion

We have introduced the programmable TMS system, which uses a pulse width modulation technique to generate flexible and stable magnetic stimuli to actuate the nervous system. The implemented TMS device has two key advantages. First, the production of consecutive rectangular pulses with a predetermined time interval, widths and polarities, enables the synthesis of a wide range of TMS waveforms. Consequently, the limitations of previous devices in the production of near-rectangular pulses or harmonic cosines are largely addressed. Second, using the PWM technique, it is possible to generate different levels of stimulus voltage from a single link DC voltage. Therefore, an efficient solution to the complexity of producing different levels of stimulus current is achievable. The stimulus polarity can be adjusted in either orientation without requiring manual mechanical coil intervention. These advantages are supported by the circuit-level implementation. The use of large capacitors allowed for the generation of constant stimulus pulses and minimized stimulus voltage decay. The stabilized voltage makes it possible to generate consistent monophasic and biphasic TBS and QPS stimulation modalities.

In summary, this paper demonstrates that generic, highly flexible pulse width modulation techniques and readily-available off-the-shelf IGBT modules can be applied in the context of high-performance TMS systems. Whilst the experimental system presented here is a laboratory prototype that does not reach the peak MSO of all devices on the market today, the proposed system is easily scaled through the addition of parallel-connected IGBT modules. We note that, even in the current form, the prototype exceeds the pulse-rate capabilities of all commercially available systems. The benefits arising from highly flexible waveform generation should enable new approaches to minimally invasive brain stimulation research and therapies.

Acknowledgment

The authors would like to thank Magstim Company Ltd (UK) for providing the stimulation coil, Magstim Rapid^2 systems, valuable guidance on design considerations, and an MRC iCASE fellowship for Karen Wendt.

References

[1] M. Chen, C. C. Cline, and K. L. Frost, "Chapter 11 - Advances and challenges in transcranial magnetic stimulation (TMS) research on motor systems," in *Engineering in Medicine, Advances and Challenges*, Orlando, FL, USA: Academic Press, 2019, pp. 283–318.
[2] D. Blumberger *et al.*, "Effectiveness of theta burst versus high-frequency repetitive transcranial magnetic stimulation in patients with depression (THREE-D): A randomised non-inferiority trial," *Lancet*, vol. 391, no. 10131, pp. 1683–1692, Apr. 2018.

[3] L. Jean-Pascal, "Chapter 37 - Transcranial magnetic stimulation," in *Handbook of Clinical Neurology*. New York, NY, USA: Elsevier B.V., 2019, pp. 559–580.

[4] A. V. Peterchev, R. Jalinous, and S. H. Lisanby, "A transcranial magnetic stimulator inducing near-rectangular pulses with controllable pulse width (cTMS)," *IEEE Trans. Biomed. Eng.*, vol. 55, no. 1, pp. 257–266, Jan. 2008.

[5] A. V. Peterchev, D. L Murphy, and S. H Lisanby, "Repetitive transcranial magnetic stimulator with controllable pulse parameters," *J. Neural Eng.*, vol. 8, no. 3, Art. no. 036016, 2011.

[6] A. V. Peterchev *et al.*, "Controllable pulse parameter transcranial magnetic stimulator with enhanced circuit topology and pulse shaping," *J. Neural Eng.*, vol. 22, no. 5, pp. 1–11, 2014.

[7] N. Gattinger, G. Moßnang, and B. Gleich, "flexTMS-a novel repetitive transcranial magnetic stimulation device with freely programmable stimulus currents," *IEEE Trans. Biomed. Eng.*, vol. 59, no. 7, pp. 1962–70, Jul. 2012.

[8] S. M. Goetz *et al.*, "Circuit topology and control principle for a first magnetic stimulator with fully controllable waveform," in *Proc. Annu. Int. Conf. IEEE Eng. Med. Biol. Soc.*, pp. 4700–4703, 2012.

[9] M. Memarian Sorkhabi *et al.*, "Deep-Brain transcranial stimulation: A novel approach for high 3-D resolution," *IEEE Access*, vol. 5, pp. 3157–3171, 2017.

[10] P. Marian, "CHAPTER 5 - Control of PWM inverter-fed induction motors," in *Control in Power Electronics, Selected Problems*. New York, NY, USA: Academic Press, 2002, pp. 161–207.

[11] M. Rosa-Clot and G. M. Tina, "Chapter 3 - Introduction to PV Plants," in *Submerged and Floating Photovoltaic Systems, Modelling, Design and Case Studies*. New York, NY, USA: Academic Press, 2018, pp. 33–64.

[12] W. Gerstner *et al.*, *Neuronal Dynamics: From Single Neurons to Networks and Models of Cognition*. Cambridge, U.K.: Cambridge Univ. Press, 2014.

[13] Z.-D. Deng, S. H. Lisanby, and A. V. Peterchev, "Electric field strength and focality in electroconvulsive therapy and magnetic seizure therapy: A finite element simulation study," *J. Neural Eng.*, vol. 8, no. 1, 2011, Art. no. 016007.

[14] S. Jezernik, T. Sinkjaer, and M. Morari, "Charge and energy minimization in electrical/magnetic stimulation of nervous tissue," *J. Neural Eng.*, vol. 7, no. 4, pp. 1–15, Jun. 2010.

[15] A. Barker, C. Garnham, and I. Freeston, "Magnetic nerve stimulation: The effect of waveform on efficiency, determination of neural membrane time constants and the measurement of stimulator output," *Electroencephalogr. Clin. Neurophysiol. Suppl.*, vol. 43, pp. 227–37, 1991.

[16] K. Sang Hoon, "Chapter 7 - Pulse width modulation inverters," in *Electric Motor Control*. New York, NY, USA: Elsevier, 2017, pp. 265–340.

[17] N. Vázquez and J. V. López, "Inverters," in *Power Electronics Handbook (Fourth Edition)*. Oxford, U.K.: Butterworth-Heinemann, 2018, pp. 289–338.

[18] B. Wu and M. Narimani, "Other multilevel voltage source inverters," in *High-Power Converters and AC Drives*. Hoboken, NJ, USA: Wiley-IEEE Press, 2017, pp. 185–223.

[19] B. Wu and M. Narimani, "Chapter 7- cascaded H-Bridge multilevel inverters," in *High-Power Converters and AC Drives*. Hoboken, NJ, USA: Wiley-IEEE Press, 2017, pp. 119–141.

[20] D. Z. Gao and K. Sun, "DC–AC inverters," in *Electric Renewable Energy Systems*. New York, NY, USA: Academic press, 2016,, pp. 354–381.

[21] B. Wu and M. Narimani, "Two-Level voltage source inverter," in *High-Power Converters and AC Drives*. Hoboken, NJ, USA: Wiley-IEEE Press, 2017, pp. 93–117.

[22] C. E. Corthout, A. Barker and A. Cowey, "Transcranial magnetic stimulation, Which part of the current waveform causes the stimulation?," *Exp. Brain Res.*, vol. 141, p. 128–132, Sep. 2001.

[23] H. Li *et al.*, "Modeling and analysis on overall fatigue," *IEEE Trans. Electron. Devices*, vol. 66, no. 3, pp. 1435–1443, Mar. 2019.

[24] M. Trivedi and K. Shenai, "Failure mechanisms of IGBT's under short-circuit," *IEEE Trans. Power Electron.*, vol. 14, no. 1, pp. 108–116, Jan. 1999.

[25] Y. Tang and H. Ma, "Dynamic electrothermal model of paralleled IGBT modules with unbalanced stray parameters," *IEEE Trans. Power Electron.*, vol. 32, no. 2, pp. 1385–1399, Feb. 2017.

[26] B. B. Jayant, "Chapter 7 - Gate drive circuit design," in *The IGBT Device*. USA: William Andrew, 2015, pp. 193–203.

[27] J. Lei *et al.*, "A health monitoring method for bond wires in IGBT modules based on voltage ringing characteristics," *IEEE Trans. Electron. Devices*, vol. 66, no. 9, pp. 3953–3960, Aug. 2019.

[28] B. B. Jayant, "Safe operating area design," in *The IGBT Device*. USA: William Andrew, 2015, pp. 117–145.

[29] J. O. Nieminen, L. M. Koponen, and R. J. Ilmoniemi, "Experimental characterization of the electric field distributioninduced by TMS devices," *Brain Stimulation*, vol. 8, no. 3, pp. 582–589, May/Jun. 2015.

[30] M. Memarian Sorkhabi *et al.*, "Measurement of transcranial magnetic stimulation resolution in 3-D spaces," *Measurement*, vol. 116, pp. 326–340, 2018.

[31] A. Peterchev *et al.*, "Pulse width dependence of motor threshold and input–output curvecharacterized with controllable pulse parameter transcranial-magnetic stimulation," *Clin. Neurophysiol.*, vol. 124, no. 7, pp. 1364–72, 2014.

[32] Q. Feng, A. D. Wu, and N. Schweighofer, "Fast estimation of transcranial magnetic stimulation motor threshold," *Brain Stimulation*, vol. 4, no. 1, pp. 50–57, 2011.

[33] Z. D. Jonker *et al.*, "TMS motor mapping: Comparing the absolute reliability of digital reconstruction methods to the golden standard," *Brain Stimulation*, vol. 12, no. 2, pp. 309–313, 2019.

[34] J. B. Pitcher, K. M. Ogston, and T. S. Miles, "Age and sex differences in human motor cortex input–output characteristics," *J. Physiol.*, vol. 546, no. 2, pp. 605–613, 2003.

[35] K. D'Ostilio *et al.*, "Effect of coil orientation on strength-duration time constant and I-wave activation with controllable pulse parameter transcranial magnetic stimulation," *Clin. Neurophysiol.*, vol. 127, no. 1, pp. 675–683, 2016.

[36] C. A. Hanlon *et al.*, "Chapter 22 - Brain stimulation as an emerging treatment for addiction," in *Cognition and Addiction*. New York, NY, USA: Academic Press, 2020, pp. 295–302.

[37] D. Gilbert, "Chapter 4 - Therapeutic rTMS in children," in *Pediatric Brain Stimulation*. New York, NY, USA: Academic Press, 2016, pp. 71–83.

[38] M. Hamada *et al.*, "Bidirectional long-term motor cortical plasticity and metaplasticity induced by quadripulse transcranial magnetic stimulation," *J. Physiol.*, vol. 586, no. 16, pp. 3927–47, Aug. 2008.

[39] H. Matsumoto and Y. Ugawa, "Quadripulse stimulation (QPS)," *Experimental Brain Res.*, Vol. 238, pp. 1619–1625, Mar. 2020.

[40] J. Voigt, L. Carpenter, and A. Leuchter, "A systematic literature review of the clinical efficacy of repetitive transcranial magnetic stimulation (rTMS) in non-treatment resistant patients with major depressive disorder," *BMC Psychiatry*, vol. 19, no. 13, pp. 1–11, 2019.

[41] N. Gattinger *et al.*, "Transcranial magnetic stimulation devices for biphasic and polyphasic ultra-high frequency protocols," *Biol. Eng. Med.*, vol. 3, no. 1, pp. 1–8, 2018.

[42] E. Babaei, "Optimal topologies for cascaded sub-multilevel converters," *J. Power Electron.*, vol. 10, no. 3, pp. 251–261, 2010.